Journal of Materials Chemistry C

PAPER

View Article Online
View Journal | View Issue

Cite this: J. Mater. Chem. C, 2018, 6, 2996

Self-standing and shape-memorable UV-curing epoxy polymers for three-dimensional (3D) continuous-filament printing†

H. Sun,[a] Y. Kim,[b] Y. C. Kim,[a] I. K. Park,[b] J. Suhr,[abc] D. Byun,[c] H. R. Choi,[c] K. Kuk,[d] O. H. Baek,[d] Y. K. Jung,[d] H. J. Choi,[e] K. J. Kim[f] and J. D. Nam*[ab]

Received 25th October 2017,
Accepted 31st January 2018

DOI: 10.1039/c7tc04873d

rsc.li/materials-c

In the development of three-dimensional printable materials for high-speed and high-resolution printing, UV-curing polymers can guarantee fast and precise printing of high performance load-bearing structures, but the injected drops of the monomers tend to spread over the substrates due to their low viscosity. In this study, we imposed the self-standing and shape-memorable capability of an epoxy acrylate (EA) monomer to ensure continuous filamentary 3D printing while maintaining its low viscosity nature. Using octadecanamide (ODA) with EA, strong hydrogen-bond networks (–N–H···O=C–, –N–C=O···H–O–, –N–H···N–) were additionally achieved in the material system and the developed material distinctively exhibited rheological duality at different processing stages: a low-viscosity liquid-like behavior (viscosity of ~50 Pa) while passing through the nozzle and a self-standing solid-like behavior (static yield stress of ~364 Pa) right after being printed. This reversible liquid-to-solid transitional capability was quantified by viscoelastic complex moduli provided a dynamic yield stress ($\tau_{y,G}$) of 210 Pa corresponding to the upright stacking up to ~3.2 cm (3 wt% of ODA). The time ($t_{y,G}$) required for conformational rearrangement was evaluated to be as fast as $\sim 10^{-2}$ s. After UV curing, the 3D printed layers exhibited no air pockets or weld lines at the stacked interfaces, which could guarantee excellent mechanical performance and structural integrity.

Introduction

Three-dimensional (3D) printing is a promising fabrication technology that attracts a great deal of attention in manufacturing fields ranging from aerospace and automotive to bioengineering.[1–4] This additive manufacturing method offers almost unlimited and unconstrained structures in a customized way without using molds, which can hardly be achieved by the traditional subtractive manufacturing technology.[5–9] As 3D printing becomes more and more central in small-scale manufacturing fields, versatile 3D-printable inks are urgently needed for achieving not only feasible processing characteristics for fast printing but also robust structural properties for being used in load-bearing structures.[10–12] Currently, 3D printing methods may be classified into two main categories in light of feedstock materials: continuous-filament and drop-jetting 3D printing.

Continuous-filament printing commonly uses thermoplastic polymers as a feedstock. It allows rapid fabrication of 3D structures (*ca.* 5–15 cm h^{-1} in the *Z*-axis), where the extruded filaments quickly solidify to construct shapes.[13] However, the viscosity of its feedstock thermoplastics is usually high in the printing region of shear rate (*e.g.*, $\sim 10^3$ Pa for PLA), which inevitably requires a large nozzle diameter (>250 μm) resulting in poor resolution of final products.[14,15] On the other hand, drop-jetting 3D printing usually adopts low-viscosity thermosetting monomers (most commonly UV-curable acrylates), which desirably allow a small nozzle size and high-resolution printing. However, the jetted droplets of thermoset monomers (1–5 μm diameter droplets) usually tend to spread over the substrate resulting in poor stacking capability (*i.e.*, low aspect ratio of the injected drops) and low printing speeds (~3 cm h^{-1} in the *Z*-axis in commercial machines).[16–19] Accordingly, if an upright standing capability is imposed to these thermoset monomers, continuous-filamentary printing could be ensured

[a] Department of Energy Science, Sungkyunkwan University, Suwon 16419, Republic of Korea. E-mail: jdnam@skku.edu
[b] School of Chemical Engineering, Department of Polymer Science and Engineering, Sungkyunkwan University, Suwon 16419, Republic of Korea
[c] Department of Mechanical Engineering, Sungkyunkwan University, Suwon 16419, Republic of Korea
[d] DMC R&D Center, Samsung Electronics Co, Ltd, Seoul 06765, Republic of Korea
[e] Department of Polymer Science and Engineering, Inha University, Incheon 22212, Republic of Korea
[f] Department of Mechanical Engineering, University of Nevada, Las Vegas, 4505 S. Maryland Parkway, Las Vegas, NV 89154, USA

† Electronic supplementary information (ESI) available. See DOI: 10.1039/c7tc04873d

in the 3D printing of thermoset monomers, which may not only overcome the poor stacking capability of drop-jetting 3D printing but also achieve a higher resolution than continuous-filament printing. Our work, therefore, focuses on ensuring continuous-filament printing using a thermoset-monomer feedstock, which allows a small nozzle size and high printing speed.

Recent work has focused on controlling the rheological behaviours of 3D printing materials to apply the desired methods including continuous-filament and drop-jetting 3D printing. In particular, for direct-write printing, shear-thinning inks were utilized due to different rheological responses by the extent of physical stimuli such as shear stress.[20,21] These fluids possessing self-standing and shape-memorable features have been classified as yield-stress fluids (or Bingham plastic fluids),[22–25] which are often observed in mayonnaise, ketchup, whipping cream, toothpaste, *etc.* They behave like a solid under quiescent conditions but flow like an ordinary liquid when a certain level of stress (*i.e.*, yield stress) is applied.[26–28] For thermoset monomers, the yield-stress characteristics may be imposed by adopting a hydrogen-bonding network in the fluids. The hydrogen-bonding network can lead to the formation of skeletal structures in thermoset monomers to maintain its shape against gravity, which is represented by yield stress. This reversible self-assembly feature of hydrogen-bonding can be used in the strategy of implementing yield-stress characteristics resulting in phase transition between the liquid-like and solid-like states within several seconds.[29–32] Hydrogen bonding can be induced using the functional groups between hydrogen attached to electro negative atoms (*e.g.*, N, O, F) and electron donators such as carbonyl oxygen (C═O). The self-assembled hydrogen-bonding skeletal structure allows the printed structure to maintain its shape against gravity and simultaneously be crumbled with ease by an external shear force or agitation.[33] Accordingly, if this yield-stress capability is imposed to a high-performance thermosetting monomer, most likely epoxy resins, a novel 3D-printing feedstock can be developed, which can flow through the printing nozzle or connection tubes with ease at a very low viscosity, but behave like a solid immediately after being printed.[34–36]

As used in this study, epoxy resins are widely considered as one of the low-viscosity (*ca.* 5–50 Pa) and high-performance thermosetting polymers used in a variety of engineering applications due to their superior mechanical properties, thermal and dimensional stability, chemical resistance and ease of processing.[37–40] Particularly, it should be noted that the UV-curable acrylated (–CH_2═CHCOO–) epoxy has both electron acceptors and donors for hydrogen bonding, corresponding to hydrogen (C–OH) and carbonyl oxygen (C═O), respectively, as schematically depicted in Fig. 1A. In order to induce a strong hydrogen-bond network, as used in this study (Fig. 1B), amides can be additionally used as an appropriate self-assembly agent because they contain both electron acceptors (NH) and donors (C═O) to form networks by itself and with epoxy acrylates, *e.g.*, N–H···O═C. It is important to choose a self-assembly agent with appropriate chain lengths and an equivalent molecular weight of NH, each influencing the speed and strength of the hydrogen-bond network. Compared with other chemicals, we carefully selected octadecanamide (ODA) as a self-assembly agent composed of 17 aliphatic –C–C– chains (~2.4 nm) containing amide groups corresponding to an equivalent molecular weight of 141.7 g eq^{-1}, which is compatible with epoxy acrylates and exhibits appropriate rheological behaviours under printing conditions exerting a strong yield-stress behaviour. This epoxy/self-assembly agent system can guarantee low-viscosity, UV-curable, and self-assembly characteristics as a yield-stress fluid, which subsequently makes it as an ideal 3D printing feedstock ensuring a versatile additive manufacturing method.

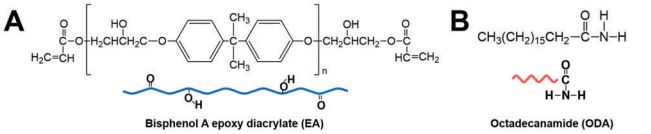

Fig. 1 Chemical structures of bisphenol A type epoxy diacrylate (A) and octadecanamide (B) and their schematic representations used in this study.

In this study, we propose a novel epoxy acrylate system including amide as a self-assembly agent exhibiting solid–liquid reversible responses that ensure 3D continuous-filament printing. The rheological characteristics of the developed material were thoroughly investigated under static and dynamic conditions identifying yield stress, viscosity, phase-transition speed, and allowable height for stacking. The self-standing and shape-memorable capability of the materials was clearly demonstrated by printing a stacked structure in the *z*-direction.

Experimental

Materials

A bisphenol A type epoxy diacrylate resin (EA) with a molecular weight of 500 g mol^{-1} and 2,4,6-trimethylbenzoyl diphenyl phosphinoxide (TPO) were purchased from ENTIS (South Korea). 1,6-Hexanediol diacrylate (HDDA) and octadecanamide (ODA) were purchased from Sigma-Aldrich and Arkema, respectively. TPO was used as a photoinitiator, which has a maximum UV absorbance at 395 nm. HDDA and ODA were used as a diluent material and a self-assembly agent, respectively. In particular, compared with our material system, polydimethylsiloxane (PDMS) was used as a reference material that has a high viscosity of ~10^5 Pa without yield stress (purchased from TA instruments, silicone standard #700.01011). As seen in Fig. 1, EA has potential hydrogen bond sites (O–H and C═O) and ODA has three potential hydrogen bond sites (two N–H and one C═O). 30 g of EA was mixed with 10 g of HDDA and vigorously stirred using a mechanical stirrer and 1 wt% of TPO was added. 1 wt% and 3 wt% of ODA were added to the neat EA, each corresponding to the droplet and continuous-filament shape, respectively. Although not included here, the extrudate at 2 wt% of ODA exhibited a state in the middle of these two representative states at 1 and 3 wt%, and there was no significant change in the shape of extrudates when the ODA composition was over 3 wt%. Three different concentrations, 0, 1 and 3 wt% of ODA in the neat EA, were referred to as neat EA, EA/ODA1 and EA/ODA3, respectively, for the study of continuous-filament 3D printing.

Characterization

The rheological characteristics were investigated using a rotational rheometer (MCR 300, Physica, Germany) equipped with a parallel plate geometry (disk diameter: 20 mm, gap size: 1 mm). Flow sweep tests were carried out at shear rates from 10^{-2} to 10^{2} s^{-1}. Dynamic oscillatory tests were performed with increasing oscillation amplitude up to 100% at a frequency of 1 Hz. Frequency sweep experiments (0.01–100 Hz) were performed at 1% strain. 3-Step interval thixotropy experiments were conducted in three oscillation steps: the samples were subjected to a strain of 0.01%, subsequently a strain of 10% was applied and as a final step 0.01% strain was implemented. The duration of each step was 60, 30 and 60 s, respectively. All the measurements were performed at 25 °C. The optical images of the extruded features were captured using a CCD camera.

Printing

The 3D printing machine (NP-expert, Enjet Inc.) employed in this study was designed to control the movement of the substrate stage in the *X*–*Y* axis and the nozzle in the *Z*-axis using a computer software. A micro-syringe pump (Harvard, new PHD Ultra™ nanomite) was used to supply the prepared inks from a syringe (1 ml) into a stainless nozzle (21G: I.D. of 0.51 mm and O.D. of 0.80 mm). The flow rate was maintained as 15 μl min^{-1}. The detailed equipment and printing conditions are reported elsewhere.[41] To build up 3D structures, the nozzle is located on a desired position and the ink deposition is commenced by working of the pump. After stacking one layer of the desired feature, the nozzle is raised up to a constant height. When the final height is reached, the ink deposition is stopped and the nozzle is vertically lifted up in order to disconnect the 3D printed structure.

Results and discussion

Fig. 2A shows the liquid state of neat EA and the solid-like state of EA/ODA, where ODA imparts yield stress to the neat EA to become a solid-like state due to the molecular skeletal structure formed through hydrogen bonding. Low-viscosity neat EA flows toward the tiling direction, while EA/ODA exhibits no flow against the gravity force. Fig. 2B shows a state in the middle of printing, where EA/ODA is stacked in three layers. In this printing, the EA/ODA shows two different stages each corresponding to a liquid-like state inside the nozzle and a solid-like state right after being printed in the stacked feature. When the ink is inside the nozzle, the shear rate or shear stress is applied to EA/ODA, which breaks the hydrogen-bonding network between the ODA and EA molecules, resulting in a low-viscosity liquid at around ~50 Pa. After the ink is printed out of the nozzle, however, molecular assembly quickly occurs to

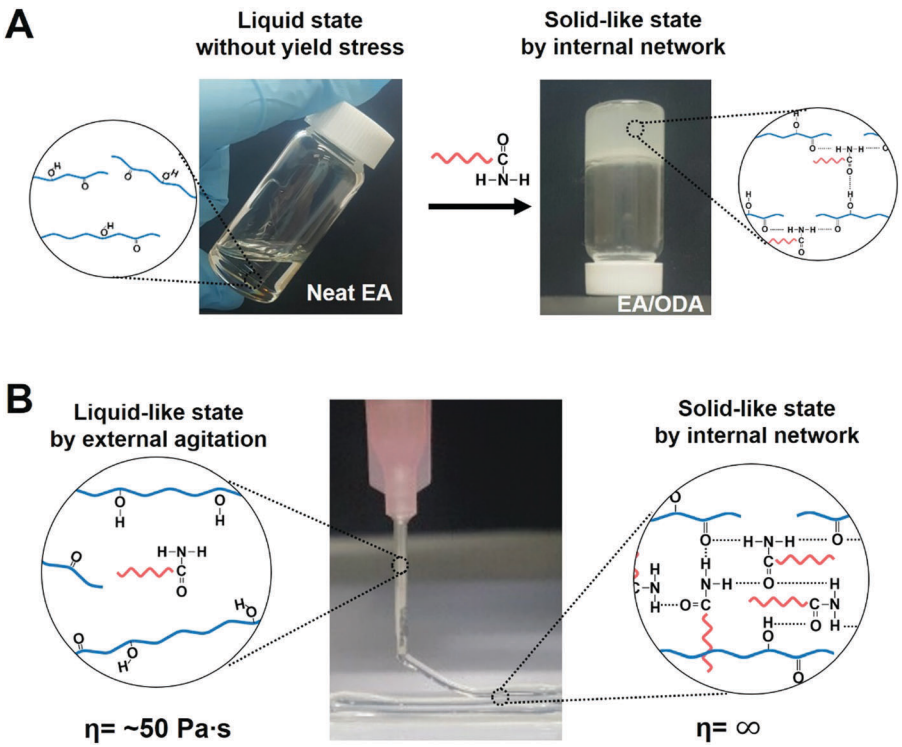

Fig. 2 Digital images of the liquid state of neat EA and the solid-like state of EA/ODA (A). The liquid state of EA is changed by adding ODA exhibiting two distinctively different states. EA and ODA are designed to form the intermolecular network structure by hydrogen-bond formation among the functional groups of the EA and ODA molecules: (EA)═O···H–N–(ODA). EA/ODA behaves as the liquid-like state (η = 50 Pa) flowing through the nozzle and the solid-like state ($\eta = \infty$) after being printed on the substrate stacked layer-by-layer without being collapsed (B). Two different states of inks result from the level of applied shear rates or shear stresses.

such an extent as to maintain the filamentary feature, and the printed parts become a solid-like state at infinity viscosity to maintain the shape of the extruded filaments against gravity force.[42] This reveals that EA/ODA exhibits a typical behaviour of yield stress fluids caused by molecular self-assembly *via* hydrogen bonding. This liquid–solid transition of the ink could be quite advantageous as a 3D printing material offering a low viscosity ink inside the nozzle and an infinity viscosity extrudate constructing self-standing 3D-printed structures. This facilitates the EA/ODA to pass through the syringe nozzle and rapidly solidify, which reveals the self-standing and shape-memorable capability.

Fig. 3A and B depict the apparent viscosity (η) and the shear stress (τ) as a function of shear rate ($\dot{\gamma}$) over 10^{-2}–10^{2} s^{-1} compared to neat EA, EA/ODA1, EA/ODA3 and PDMS. In Fig. 3A, the viscosities of the EA/ODA specimens (EA/ODA1 and EA/ODA3) are lower than that of PDMS, which is a reference material exhibiting a typical pseudoplastic behaviour, in the entire shear-rate range. Their viscosities continue to decrease fast with the increase of $\dot{\gamma}$, which suggests that our ink system is the thixotropic fluid that exhibits variable viscosities with respect to shear rate. For example, the viscosity of EA/ODA3 is decreased to $\sim 10^{2}$ Pa, which is substantially lower than $\sim 10^{4}$ Pa of PDMS both measured at 10 s^{-1}. It is clear that the EA/ODA specimens are more advantageous than PDMS for printing through the fine nozzles due to their lower viscosities than PDMS. In the logarithmic plots τ *vs.* $\dot{\gamma}$ (Fig. 3B), the neat EA ink shows a typical Newtonian fluid behaviour exhibiting a linear increment of τ with $\dot{\gamma}$, and τ of PDMS is increased without a plateau region. On the other hand, τ of EA/ODA specimens clearly shows a typical yield-stress fluid behaviour exhibiting a constant τ with an increase of $\dot{\gamma}$, which demonstrates the presence of "static yield stress (τ_y)," *i.e.*, a shear-stress plateau as $\dot{\gamma} \rightarrow 0$.

Herein, the yield stress can be obtained by the extrapolation of shear stress to the zero shear rate region. Yield-stress fluids or Bingham fluids have been described by the Herschel–Bulkley model (H–B model) as follows:[43]

$$\tau = \tau_y + K\dot{\gamma}^n \quad (1)$$

where K is the consistency factor and n is the flow behavior index. Analyzing the results in Fig. 3B based on eqn (1), it can be seen that the H–B model compares well the experimental results of neat EA and EA/ODA specimens with the model parameters summarized in Table 1. PDMS is not applicable for the H–B model. EA/ODA1 and EA/ODA3 give τ_y of 71.6 Pa and 364 Pa, respectively, which should be compared with that of 0 Pa for neat EA. When we assume that gravity is only applied to the printed structure of yield stress fluids, the structure can withstand its own weight against gravity by the quantification of yield stress and its theoretical height can be estimated, *viz*:[26]

$$h = \frac{\tau_y}{\rho g}. \quad (2)$$

where h is the theoretical height, ρ is the density of the yield stress fluids and g is the acceleration due to gravity. Using eqn (2), h of the extruded filaments of EA/ODA3 is estimated to be 3.2 cm, which is the visualized upright capacity corresponding to a yield stress (τ_y) of 364 Pa. It should be compared with the yield stresses of materials such as mayonnaise, ketchup and tooth paste corresponding to yield stresses of 100, 30, and 215 Pa, respectively. In other words, the extruded filaments can be overlaid repeatedly up to that height without spreading or collapsing by gravity without any solidification steps. In practical printing processing, the overlaid structure is usually solidified *in situ* by UV curing subsequently extending the theoretical heights of inks.

The yield-stress characteristics may be confirmed by observing the extrudate shapes changing with time after being printed. In Fig. 3C and D, the height of PDMS, whose viscosity is much higher than that of EA/ODA, decreases by nearly 20% after 5 min. After 30 min, PDMS collapses by nearly 70%, spreading over the substrate. On the other hand, EA/ODA3 maintains its initial shape and height, where the spreading phenomenon is not observed even after 30 min. By imposing yield-stress characteristics to EA, it is demonstrated that the low-viscosity epoxy can be used as a feedstock for 3D continuous-filament printing device in a way of stacking the filaments just like high-viscosity thermoplastic polymers.

The gravitational spreading phenomenon of a high-viscosity drop may be evaluated as a function of time assuming that the drop flows by the gravity force in the quasi-steady state:[44]

$$\frac{h_t}{h_0} = \frac{0.531}{h_0}\left(\frac{3vV}{gt}\right)^{1/4} \quad (3)$$

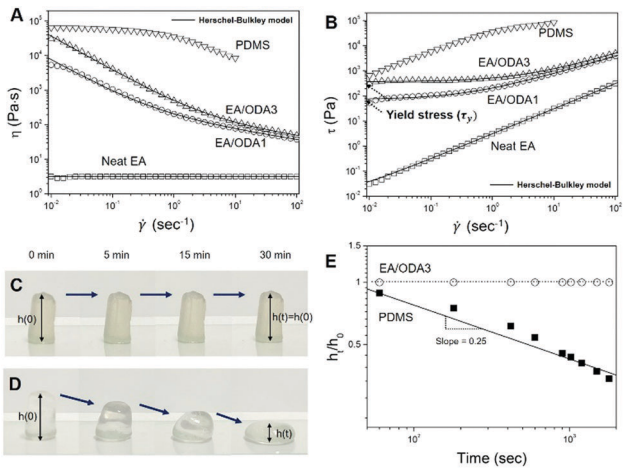

Fig. 3 The rheological characteristics of the neat EA, EA/ODA1, EA/ODA3 and PDMS: apparent viscosity (A) as functions of shear rate and shear stress (B) as a function of shear rate compared with the Herschel–Bulkley model description (solid lines). Digital images of extrudates of PDMS (C) and EA/ODA3 (D), whose heights are plotted as a function of time in (E).

Table 1 The parameters (τ_y, K, and n) of the Herschel–Bulkley model, theoretical height (h) and dynamic yield stress ($\tau_{y,G}$) for neat EA, EA/ODA1 and EA/ODA3

	τ_y (Pa)	K	n	h (cm)	$\tau_{y,G}$ (Pa)
Neat EA	0	3.13	0.999	0	—
EA/ODA1	71.6	138	0.714	0.6	40
EA/ODA3	364	150	0.746	3.2	210

where h_t is the transient height, h_0 is the initial height, ν is the kinematic viscosity, V is the volume of the drop, and t is the time. eqn (3) describes well the experimental results of PDMS as seen in Fig. 3E, where h_t decreases in proportion to $t^{-1/4}$. Compared with the collapsing PDMS, it is clearly seen that EA/ODA3, which is a yield-stress fluid, maintains the initial height against the gravity force regardless of time. This proves that EA/ODA3 exhibits the self-standing and shape-memorable capability that could substantially increase the printing speed and resolution by such rapid stabilization of the printed structures.

In this study, the phase transition of our ink systems between the solid-like and liquid-like states is clearly demonstrated by analysing the viscoelastic properties each corresponding to the storage modulus (G') and loss modulus (G'') of materials. When G' is higher than G'', the material is predominantly in the solid-like state and *vice versa*. In this sense, the crossover points of G' and G'' can be attributed to the transition from the solid-like to the liquid-like states, which may very well correspond to the yield point of the material. In the oscillatory experiments, G' and G'' of the EA/ODA specimens and PDMS are plotted as a function of τ as shown in Fig. 4A. EA/ODA1 and EA/ODA3 show that G' is maintained higher than G'' up to crossover points of 40 Pa and 210 Pa, respectively, followed by the region, where G'' is higher than G'. The obtained crossover points in Fig. 4A provide dynamic yield stresses ($\tau_{y,G}$) of EA/ODA1 and EA/ODA3, which agree well with τ_y at 71.6 and 364 Pa as shown in Table 1, respectively. When the ink flows through a nozzle, the wall shear stress under our experimental conditions is estimated to be 1825 Pa for EA/ODA3,[45,46] which is higher than the yield stress ($\tau_{y,G}$ at 364 Pa) of our material. This supports that EA/ODA3 should flow in the liquid-like state inside the nozzle at 50 Pa (Fig. 3A). However, when the ink is extruded out of the nozzle as a filament, the applied shear stress becomes nearly zero, which turns it into a solid-like state. It can be further analysed using $\tan\delta$ (G''/G'), which quantifies elastic or viscous contributions under borderline conditions of the phase transition at $\tan\delta = 1$. Fig. 4B shows $\tan\delta$ of EA/ODA specimens and PDMS as a function of τ. The $\tan\delta$ of EA/ODA specimens increases with τ passing through the borderline at $\tan\delta = 1$ representing a liquid-like behaviour in the low shear-stress region and a solid-like behaviour in the high shear-stress region. It is clear that the shear stress at $\tan\delta = 1$ is consistent with $\tau_{y,G}$ as measured in Fig. 4A. On the other hand, the $\tan\delta$ of PDMS is 1.0 in the entire region. The time ($t_{y,G}$) required for the reversible liquid-to-solid transition may be evaluated by frequency-sweep tests. Fig. 4C shows G' and G'' of EA/ODA specimens measured as a function of frequency (f). The crossover points of EA/ODA1 and EA/ODA3 specimens are observed at f = 20 Hz and 100 Hz each corresponding to $t_{y,G} = 1/f$ = 0.01 s and 0.05 s, respectively. The crossover points of G' and G'' are related to phase transition, which may very well correspond to time required for the liquid-to-solid or solid-to-liquid transition. This time may be ascribed to the time for the EA and ODA molecules to form the skeletal network of hydrogen bonding. It should be associated with the time for hydrogen bonding kinetics, viscosity and diffusion mobility of EA monomers and ODA, and on the other hand, the hydrogen bonding has a weak effect on the mechanical properties of our ink as seen in Fig. S1, ESI.† Fig. 4D depicts the 3-step interval thixotropy test of EA/ODA specimens, which shows the typical characteristics of thixotropic fluids: the recovery of viscosity and/or moduli after the structure was broken down under changing shear rates.[47] They exhibit a G' higher than G'' at a low strain at 0.01% but it turns *vice versa* at a high strain at 10%. When a low strain is applied again, the initial value of G' is rapidly increased and recovered. The first and last regions (at low strain) show the build-up of the network structure and the middle region indicates the breakdown of the structure. This rapid and reversible response stems from molecular self-assembly *via* hydrogen bonding allowing the breakdown or reassembly of our ink system depending on the extent of deformation. In this regard, our inks have the reversible thixotropic nature, which is desired for 3D printing materials because they can easily flow through the nozzle and maintain the continuous-filament shape after extrusion.

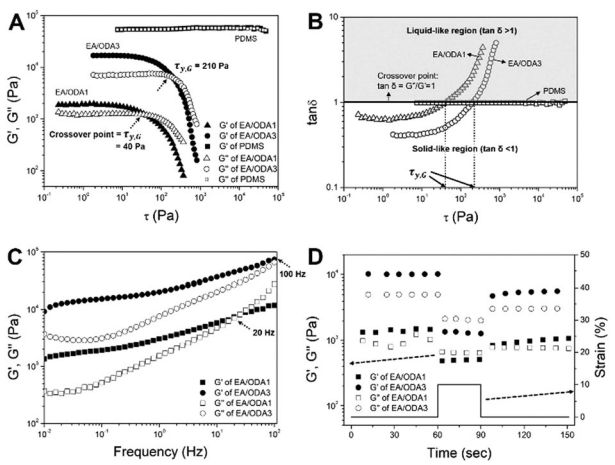

Fig. 4 Viscoelastic properties of EA/ODA1, EA/ODA3 and PDMS plotted by storage modulus, G', loss modulus, G'', (A) and $\tan\delta$ (B) as a function of shear stress. G' and G'' as a function of frequency (C) from 0.01 to 100 Hz under a constant strain of 0.1% for EA/ODA specimens. The crossover point means the time scale of phase change between the solid-like behavior and liquid-like behavior. G' and G'' as functions of three time-steps at the applied strain in a low–high–low (0.01%–10%–0.01%) fashion using a frequency of 1 Hz (D). The solid line represents the corresponding strain applied to the specimens.

Fig. 5 compares the sequential images of the low yield-stress ink (EA/ODA1) and high yield-stress ink (EA/ODA3) extruding out of the tip of the syringe needle. In general, as a spherical drop grows until the drop volume exceeds a critical weight for the drop to fall down. The maximum size of the drop held by the surface tension at the tip of the needle can be expressed by the following equation: $V_{max} = \sigma\pi D/\rho g$, where V_{max} is the maximum volume of the drop, σ is the surface tension of the liquid and D is the diameter of the nozzle.[48] In the yield-stress fluid, however, the yield stress (τ_y) is additionally exerted to hold the drop at the nozzle tip resulting in a drop in a long-neck pendent shape (Fig. 5A), whose volume is bigger than V_{max}, or a continuous-filament shape (Fig. 5B) when the yield stress is further increased. Accordingly, it is clear that the yield stress is

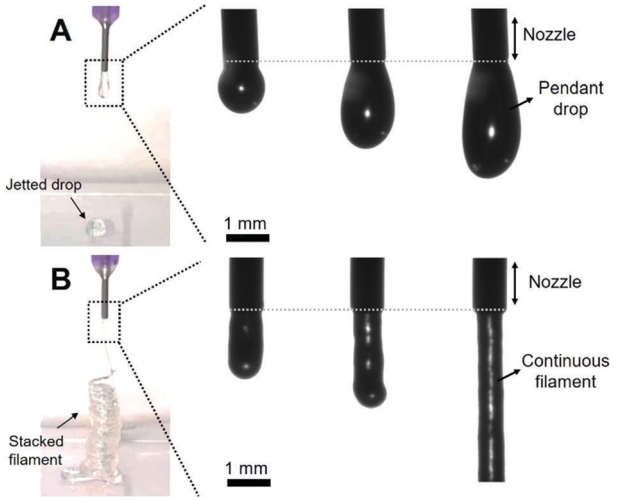

Fig. 5 Comparison of two different level yield-stress materials representing drop-jetting printing (A) and continuous-filament printing (B) each represented by sequential images of EA/ODA1 and EA/ODA3, respectively, extruded from the nozzle with an inner diameter of 500 μm. Due to the low yield stress, EA/ODA1 has a pendant drop, which is suitable for drop-jetting 3D printing. EA/ODA3 shows a continuous filamentary shape due to high yield stress, which facilitates the filamentary features and endures the stacked layers.

likely to be added to the intrinsic surface tension subsequently increasing the drop volume to surpass the gravity force resulting in shape-memorable capability (retention of the filamentary shape).

Using our high yield-stress ink (EA/ODA3), Fig. 6A demonstrates a stacked rim structure in a way of continuous-filament 3D printing. Due to high yield stress, the filaments are stacked with ease without buckling or spreading even before UV curing. When UV-cured (Fig. 6B), the printed rim structure turns yellow and becomes strong and robust maintaining its structural integrity even in such a bending deformation. Fig. 6C and D show the cross sectional images of the 5-layer printed rim after UV curing. This indicates no filamentary boundaries between the individual printed filaments demonstrating that the interfaces of the printed layers well cohered with each other, which is the quite different from the printing cases of most thermoplastic materials. In thermoplastics, the overlaid boundaries often exhibit weld-lines leaving air pockets or weak-interface lines due to the intrinsically long relaxation time (or healing time) of high-molecular polymer chains. Fig. 6E shows the height and width of the printed structures as a function of the stacking number of layers. The width is nearly constant, while their heights are linearly increased. The thickness of each layer is 520 μm, which resultantly gives a structural height of 2.6 mm by stacking up only five filaments. To demonstrate the upright capacity of our high yield-stress ink (EA/ODA3), we printed a stacked wall structure (7.5 mm) composed of 40 stacked layers in a way of continuous-filament 3D printing as shown in Fig. 6F. Fig. 6G shows a printed symbol demonstrating the capability of our ink system printing complex patterns or shapes, *e.g.*, a gingko-leaf feature, which is composed of multiple radii and sharp angles. This demonstrates that our material possesses the capability of building up 3D-printed self-standing structures without defects at the interfaces of the stacked layers, which is attributed to the monomeric components of our ink system providing the superior mechanical properties of 3D-printed structures.

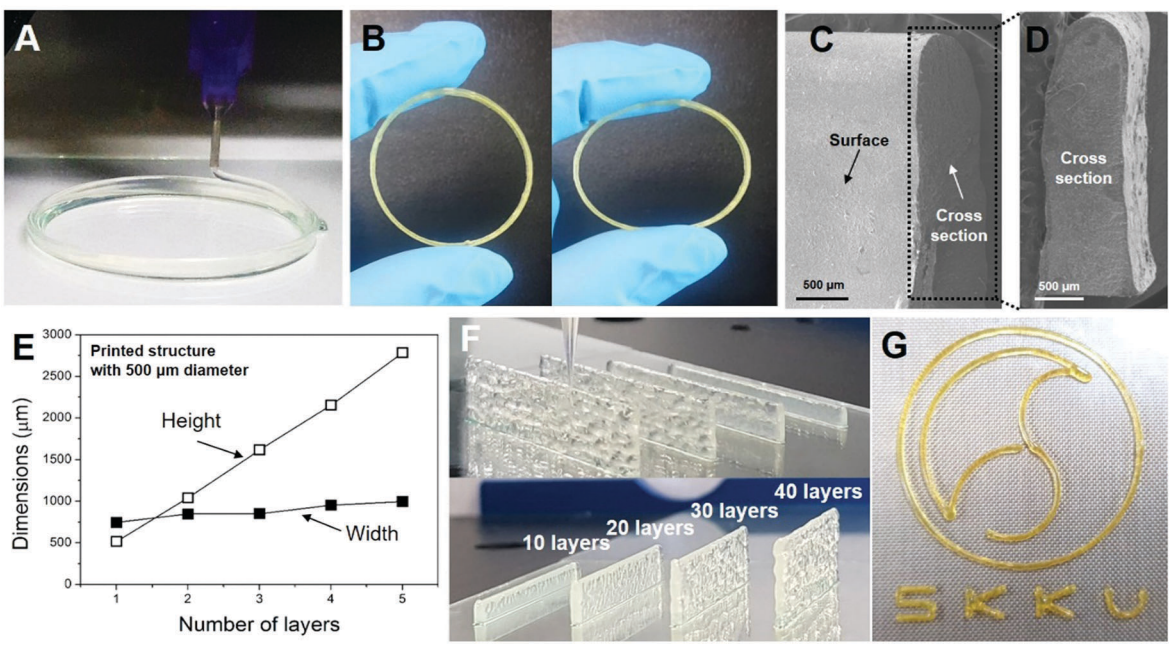

Fig. 6 Digital image of the 3D printing process of the rim structure using EA/ODA3 with a 500 μm nozzle (A). Printed rim structure after UV curing composed of five stacked filament layers (B). SEM cross-section images of the printed structure in side view in (C) and front-view in (D), the height and width of which are plotted in (E). Digital images of line structures with 10, 20, 30 and 40 layers (F) and a 3D printed gingko leaf structure (G), which is conducted using a tapered nozzle with a diameter of 200 μm.

Conclusions

In this study, we developed a novel epoxy-based resin system, which has shape-memorable and self-standing capability. The hydrogen-bond network was imposed using an appropriate amide compound. Depending on the level of yield stress, the theoretical height of the 3D printed structures could be predicted by theory and confirmed by experiments. The extrudate shape and spreading phenomenon were identified with time. Additionally, tan δ accurately demonstrated the liquid–solid phase transition under printing operation conditions. The yield stress and tan δ indicate that our high yield-stress fluid can be utilized in continuous-filament 3D printing, which could enable low-viscosity thermosetting polymer systems to exert the self-standing and shape-memorable capability.

Notes

J. D. Nam designed the experiments. H. Sun carried out the experiments and wrote the manuscript. Y. Kim, Y. C. Kim and I. K. Park contributed to data analysis. J. Suhr and D. Byun developed the overall concepts. K. Kuk, O. H. Baek and Y. K. Jung coordinated the experiments. H. J. Choi, H. R. Choi and K. J. Kim conceived the idea. All the authors reviewed the manuscript.

Conflicts of interest

There are no conflicts to declare.

Acknowledgements

This work was supported by the National Research Foundation of Korea (NRF), the Ministry of Science, ICT & Future Planning (NRF-2014M3C1B2048175, 2016R1A2B1007134, and NRF-2017R1A2B4006091), and the Ministry of Trade, Industry and Energy (MOTIE) (10067690). We also appreciate the project and equipment support from Gyeonggi Province through the GRRC program of Sungkyunkwan University. KJK would like to acknowledge the partial financial support from the US National Science Foundation (#1545875).

References

1 B. C. Gross, J. L. Erkal, S. Y. Lockwood, C. Chen and D. M. Spence, *Anal. Chem.*, 2014, **86**, 3240–3253.
2 J. M. Zhang, E. Q. Li, A. A. Aguirre-Pablo and S. T. Thoroddsen, *RSC Adv.*, 2016, **6**, 2793–2799.
3 Y. Jiang, Y. Chen, M. Zhang, Y. Qiu, Y. Lin and F. Pan, *RSC Adv.*, 2016, **6**, 51871–51876.
4 K. Fu, Y. Yao, J. Dai and L. Hu, *Adv. Mater.*, 2017, **29**, 1603486.
5 M. Faes, J. Vleugels, F. Vogeler and E. Ferraris, *CIRP Journal of Manufacturing Science and Technology*, 2016, **14**, 28–34.
6 U. Kalsoom, P. N. Nesterenko and B. Paull, *RSC Adv.*, 2016, **6**, 60355–60371.
7 Y. C. Kim, S. Hong, H. Sun, M. G. Kim, K. Choi, J. Cho, H. R. Choi, J. C. Koo, H. Moon and D. Byun, *Eur. Polym. J.*, 2017, **93**, 140–147.
8 W. Jo, J. S. Lee, H. J. Lee and M.-W. Moon, *RSC Adv.*, 2014, **4**, 31764–31770.
9 R. D. Farahani, M. Dube and D. Therriault, *Adv. Mater.*, 2016, **28**, 5794–5821.
10 M. Zhang, A. Vora, W. Han, R. J. Wojtecki, H. Maune, A. B. A. Le, L. E. Thompson, G. M. McClelland, F. Ribet, A. C. Engler and A. Nelson, *Macromolecules*, 2015, **48**, 6482–6488.
11 P. Calvert, *Chem. Mater.*, 2001, **13**, 3299–3305.
12 H. Lipson and M. Kurman, *Fabricated: The new world of 3D printing*, John Wiley & Sons, 2013.
13 N. P. Bansal and A. R. Boccaccini, *Ceramics and composites processing methods*, John Wiley & Sons, 2012.
14 X. Hao, J. Kaschta, X. Liu, Y. Pan and D. W. Schubert, *Polymer*, 2015, **80**, 38–45.
15 K. V. Wong and A. Hernandez, *ISRN Mech. Eng.*, 2012, 1–10.
16 A. Selimis, V. Mironov and M. Farsari, *Microelectron. Eng.*, 2015, **132**, 83–89.
17 J. Stringer and B. Derby, *J. Eur. Ceram. Soc.*, 2009, **29**, 913–918.
18 H. Sirringhaus, T. Kawase and R. Friend, *MRS Bull.*, 2001, **26**, 539–543.
19 C. J. Hansen, R. Saksena, D. B. Kolesky, J. J. Vericella, S. J. Kranz, G. P. Muldowney, K. T. Christensen and J. A. Lewis, *Adv. Mater.*, 2013, **25**, 96–102.
20 R. L. Truby and J. A. Lewis, *Nature*, 2016, **540**, 371–378.
21 M. Vatani, M. Vatani, J.-W. Choi and J.-W. Choi, *Rapid Prototyping J.*, 2017, **23**, 337–343.
22 E. C. Bingham, *Fluidity and plasticity*, McGraw-Hill, 1922.
23 G. Benmouffok-Benbelkacem, F. Caton, C. Baravian and S. Skali-Lami, *Rheol. Acta*, 2010, **49**, 305–314.
24 D. Bonn and M. M. Denn, *Science*, 2009, **324**, 1401–1402.
25 P. Moller, A. Fall, V. Chikkadi, D. Derks and D. Bonn, *Philos. Trans. R. Soc., A*, 2009, **367**, 5139–5155.
26 H. A. Ardakani, E. Mitsoulis and S. G. Hatzikiriakos, *J. Non-Newtonian Fluid Mech.*, 2011, **166**, 1262–1271.
27 H. A. Barnes, 2000.
28 P. C. F. Møller, J. Mewis and D. Bonn, *Soft Matter*, 2006, **2**, 274.
29 G. R. Desiraju, *Chem. Commun.*, 1997, 1475–1482.
30 K. Wendler, J. Thar, S. Zahn and B. Kirchner, *J. Phys. Chem. A*, 2010, **114**, 9529–9536.
31 J. A. Lewis and G. M. Gratson, *Mater. Today*, 2004, **7**, 32–39.
32 X. Zhou, C. Li, Y. Shao, C. Chen, Z. Yang and D. Liu, *Chem. Commun.*, 2016, **52**, 10668–10671.
33 S. R. Raghavan, H. Walls and S. A. Khan, *Langmuir*, 2000, **16**, 7920–7930.
34 A. Abbadessa, M. Blokzijl, V. Mouser, P. Marica, J. Malda, W. Hennink and T. Vermonden, *Carbohydr. Polym.*, 2016, **149**, 163–174.
35 G. M. Pawar, M. Koenigs, Z. Fahimi, M. Cox, I. K. Voets, H. M. Wyss and R. P. Sijbesma, *Biomacromolecules*, 2012, **13**, 3966–3976.
36 T. Billiet, M. Vandenhaute, J. Schelfhout, S. Van Vlierberghe and P. Dubruel, *Biomaterials*, 2012, **33**, 6020–6041.
37 N. Domun, H. Hadavinia, T. Zhang, T. Sainsbury, G. H. Liaghat and S. Vahid, *Nanoscale*, 2015, **7**, 10294–10329.

38 R. Thomas, D. Yumei, H. Yuelong, Y. Le, P. Moldenaers, Y. Weimin, T. Czigany and S. Thomas, *Polymer*, 2008, **49**, 278–294.
39 G. Pan, Z. Du, C. Zhang, C. Li, X. Yang and H. Li, *Polymer*, 2007, **48**, 3686–3693.
40 N. Chikhi, S. Fellahi and M. Bakar, *Eur. Polym. J.*, 2002, **38**, 251–264.
41 F. D. Prasetyo, H. T. Yudistira, V. D. Nguyen and D. Byun, *J. Micromech. Microeng.*, 2013, **23**, 095028.
42 P. Coussot, Q. D. Nguyen, H. T. Huynh and D. Bonn, *Phys. Rev. Lett.*, 2002, **88**, 175501.
43 W. H. Herschel and R. Bulkley, *Colloid Polym. Sci.*, 1926, **39**, 291–300.
44 S. Middleman, *An introduction to fluid dynamics: principles of analysis and design*, John Wiley & Sons Incorporated, 1998.
45 J.-F. Agassant, P. Avenas, P. J. Carreau, B. Vergnes and M. Vincent, *Polymer processing: principles and modeling*, Carl Hanser Verlag GmbH Co KG, 2017.
46 The wall stress in the Hagen-–Poiseuille equation equation is $\tau_w = \Delta PR/2L$. The experimental conditions of our printing are R = 250 μm, ΔP = 146 000 Pa and L = 1 cm, which gives τ_w = 1833 Pa.
47 J. Mewis and N. J. Wagner, *Adv. Colloid Interface Sci.*, 2009, **147**, 214–227.
48 G. K. Batchelor, *An introduction to fluid dynamics*, Cambridge University Press, 2000.